Eur. Phys. J. D **5**, 363–374 (1999)

THE EUROPEAN PHYSICAL JOURNAL D

EDP Sciences
© Società Italiana di Fisica
Springer-Verlag 1999

Fringe contrast in three grating Mach-Zehnder atomic interferometers

C. Champenois[a], M. Büchner, and J. Vigué

Laboratoire Collisions, Agrégats, Réactivité, IRSAMC, Université Paul Sabatier and CNRS[b], 118 route de Narbonne, 31062 Toulouse, France

Received: 24 April 1998 / Revised: 25 October 1998 / Accepted: 11 December 1998

Abstract. Several three-grating Mach-Zehnder atomic interferometers have been built and operated in recent years but no general theory of the contrast of the fringes produced by these apparatus is available. The purpose of this paper is to develop this theory, based on the Fresnel-Kirchoff approximate treatment of diffraction. Such a theory has been developed by Turchette *et al.* [JOSA B **9**, 1601 (1992)] but because the necessary multiple integrals were evaluated in a purely numerical way, this treatment was not fully general. We show here how to reduce the computation by analytic means and we are thus able to calculate the contrast with a modest numerical effort. Moreover, we get a simple insight of the contrast reduction related to several defects of a real apparatus. We apply our calculations to existing interferometers as well as to an apparatus working with lithium which is under construction in our laboratory.

PACS. 03.75.Dg Atom and neutron interferometry – 32.80.Lg Mechanical effects of light on atoms, molecules, and ions – 42.50.Vk Mechanical effects of light on atoms, molecules, electrons, and ions

1 Introduction

When building an atomic interferometer, one is concerned with the contrast of the fringes produced by the apparatus. The contrast depends on the source, on the tools used to create interfering beams (mirrors and beam splitters) and on the geometry of the apparatus. Our interest will be focused on atomic interferometers with spatially separated beams.

In order to optimize the interferometer we are building, we have developed a very simple numerical simulation so that we can easily vary the geometrical parameters. Throughout the present study, we focus on the geometrical effects and consider that the atoms are optically pumped into the same internal state. This pumping avoids the loss of contrast due to magnetically-induced phase shifts between the different Zeeman sub-levels [1]. Furthermore, we suppose a perfectly steady interferometer and do not take into account vibrations, acceleration and rotation of the interferometer.

In Section 2, we describe the type of atomic interferometers with which we are dealing and in Section 3, we explain the model we use to simulate them. In Section 4, we analyze the effect of misalignment on the fringe contrast and in Section 5 we emphasize the conceptual differences between amplitude gratings [2] and phase gratings [3,4] and their consequences on the contrast. We evaluate the effect of the paths corresponding to different diffraction orders on the contrast of an interferometer working with lithium and phase gratings and compare it with one already built using amplitude gratings and sodium [2]. In this section, we also discuss the possible improvements of the contrast.

2 The three grating Mach-Zehnder atomic interferometer

The atomic interferometers we are simulating are of the Mach-Zehnder type, where the mirrors and the beam splitters are three diffraction gratings. Examples of such interferometers are described in references [2,5,6] and their general design is represented in Figure 1. In such a device, the two first gratings separate the incoming beam into several paths corresponding to different diffraction orders. Some of those recombine in the plane of the last grating and interfere after diffraction by this grating. The detector, usually placed in front of the interferometer exit shown in this figure, remains fixed during data acquisition [6,7]. In atom interferometers, the source is a skimmed atomic beam collimated by two slits S_0 and S_1, usually of the same width e, which reduce the transverse velocity and angular dispersion of the beam. Three diffraction gratings G_1, G_2, G_3 are needed and the signal comes from a surface ionization detector (*i.e.* a hot wire for alkali atoms [2] or a channeltron behind a selecting slit for metastable rare gas atoms [5,6]).

[a] e-mail: caroline@yosemite.ups-tlse.fr
[b] UMR 5589

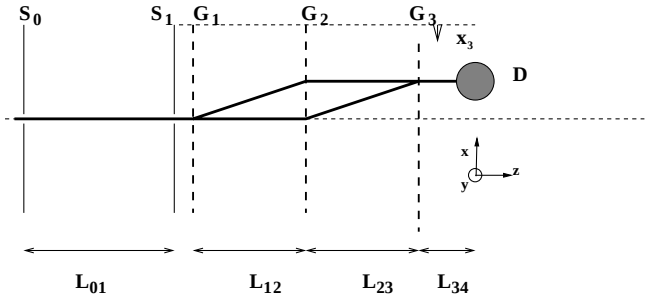

Fig. 1. Schematic drawing of an atomic interferometer of the Mach-Zehnder type. S_0 and S_1 are collimating slits of width e_0 and e_1 (typically 10 μm) and G_1, G_2 and G_3 are the three gratings. D designates the atomic detector of width d (taken equal to 50 or 100 μm in our simulations). In our simulations, we have fixed the other parameters to the values of Pritchard's experiment [2]: $L_{01} = 0.8$ m, $L_{12} = L_{23} = 0.6$ m and the distance between the slit S_1 and the first grating G_1 has been neglected. The distance L_{34} between the third grating G_3 and the detector D has been varied between 0 and 0.6 m. Only two interfering paths are represented by thick lines. The diffraction orders p_1 p_2 p_3 as defined in the text are equal to 1 -1 0 for the upper path and 0 1 -1 for the lower path.

Table 1. Relevant parameters for atomic diffraction. For sodium, material gratings have been used and $a = 200$ nm is the value given in reference [2] while for Li and Ar^*, the gratings are quasi-resonant stationary laser waves with a wavelength equal to $2a$.

atom	velocity	λ	grating period a	θ
Na	1000 m/s	0.17 Å	200 nm	87 μrad
Li	1000 m/s	0.57 Å	335 nm	170 μrad
Ar^*	850 m/s	0.12 Å	405 nm	29 μrad

A plane wave description of the propagation through the interferometer is very useful to understand how the fringes can be observed. However, as it will appear later, this description is a rough approximation for atomic waves because of diffraction by the slits. In this model, the initial atomic beam propagating along $\mathbf{z}$ axis is described by a plane wave $e^{i\mathbf{k}_a\cdot\mathbf{r}}$ ($\mathbf{k}_a \| \mathbf{z}$). A reciprocal vector $\mathbf{k}_{g_i}$ is associated with each grating G_i, $\|\mathbf{k}_{g_i}\| = 2\pi/a$ where a is the period of the grating G_i, assumed to be the same for the three gratings. As $\|\mathbf{k}_{g_i}\| \ll \|\mathbf{k}_a\|$ and $\mathbf{k}_{g_i}\cdot\mathbf{k}_a \simeq 0$, the diffracted beam which encounters a diffraction of order p_i by the grating G_i is simply expressed as $e^{i\mathbf{k}_a\cdot\mathbf{r}}e^{ip_i\mathbf{k}_{g_i}\cdot(\mathbf{r}-\mathbf{r}_i)}$. Here $\mathbf{r}_i$ defines the position of the grating G_i. The first order diffraction angle θ is defined by

$$\theta = \frac{\lambda}{a} = \frac{\|\mathbf{k}_{g_i}\|}{\|\mathbf{k}_a\|} \tag{1}$$

where λ is the atomic wavelength. Values of θ are given in Table 1 for some typical experiments.

If we consider only the two paths represented in Figure 1, the resulting amplitude is the sum of two amplitudes

$$\begin{aligned}\varphi_{1-10} &= A_{1-10}e^{i\left(\mathbf{k}_a\cdot\mathbf{r}+\mathbf{k}_{g_1}\cdot(\mathbf{r}-\mathbf{r}_1)-\mathbf{k}_{g_2}\cdot(\mathbf{r}-\mathbf{r}_2)\right)}\\ \varphi_{01-1} &= A_{01-1}e^{i\left(\mathbf{k}_a\cdot\mathbf{r}+\mathbf{k}_{g_2}\cdot(\mathbf{r}-\mathbf{r}_2)-\mathbf{k}_{g_3}\cdot(\mathbf{r}-\mathbf{r}_3)\right)}\end{aligned} \tag{2}$$

where the indices stand for successive diffraction orders p_1 p_2 p_3. In a symmetric Mach-Zehnder interferometer (if the gratings G_1 and G_3 are identical), the amplitudes A_{1-10} and A_{01-1} are equal (see Appendix C) and the intensity in the detector plane is proportional to

$$\begin{aligned}I &= |\varphi_{1-10} + \varphi_{01-1}|^2\\ &= I_0\left(1 + \cos\left((\mathbf{k}_{g_1} + \mathbf{k}_{g_3} - 2\mathbf{k}_{g_2})\cdot\mathbf{r} - \Phi\right)\right)\end{aligned} \tag{3}$$

where the phase $\Phi = (\mathbf{k}_{g_1}\cdot\mathbf{r}_1 + \mathbf{k}_{g_3}\cdot\mathbf{r}_3 - 2\mathbf{k}_{g_2}\cdot\mathbf{r}_2)$ depends only on the position of the gratings. When varying this phase Φ by, for example, shifting the last grating along $\mathbf{x}$, the intensity at point $\mathbf{r}$ varies from 0 to I_0 resulting in an interference pattern with a contrast equal to unity (the contrast is defined as usual by $C = (I_{max} - I_{min})/(I_{max} + I_{min})$). If the three gratings have the same period and the same direction, then $\mathbf{k}_{g_1} + \mathbf{k}_{g_3} - 2\mathbf{k}_{g_2} = 0$ and this pattern does not depend on the detection point, and the contrast remains equal to unity when the signal is integrated over the detector surface. As Φ is independent of the atomic wavevector, all the atoms of the beam have the same contribution to the signal, whatever their velocity. This apparatus has a "white fringe contrast".

3 The model

We develop here a model very similar to the one of Turchette *et al.* [8] but we are able to reduce considerably the numerical computation by changes of variables and analytic integrations. In this model, we consider the first collimating slit S_0 as an incoherent source. The signal measured by the detector is then proportional to the intensity I, integrated over the detector points $\mathbf{R}_4$ and the source points $\mathbf{R}_0$.

$$I = \int_{source} d\mathbf{R}_0 \int_{detector} d\mathbf{R}_4 |A(\mathbf{R}_0, \mathbf{R}_4)|^2 \tag{4}$$

where $A(\mathbf{R}_0, \mathbf{R}_4)$ is the amplitude diffracted from the source point $\mathbf{R}_0$ to the point $\mathbf{R}_4$. In the scalar theory of diffraction, this amplitude is given by the Fresnel-Kirchoff diffraction integral. If we take into account the diffraction by the second slit and first grating, assumed to be in the same plane, followed by diffraction by the last two gratings, the amplitude $A(\mathbf{R}_0, \mathbf{R}_4)$ depends on the transmission of the gratings $t_i(\mathbf{R}_i)$ as

$$\begin{aligned}A(\mathbf{R}_0, \mathbf{R}_4) = \frac{A_0}{i\lambda^3}\int_{S_1} d\mathbf{R}_1 \frac{e^{ik_a R_{01}}}{R_{01}} t_1(\mathbf{R}_1)\\ \times \int_{-\infty}^{\infty} d\mathbf{R}_2 \frac{e^{ik_a R_{12}}}{R_{12}} t_2(\mathbf{R}_2) \int_{-\infty}^{\infty} d\mathbf{R}_3 \frac{e^{ik_a R_{23}}}{R_{23}} t_3(\mathbf{R}_3) \frac{e^{ik_a R_{34}}}{R_{34}}\end{aligned} \tag{5}$$

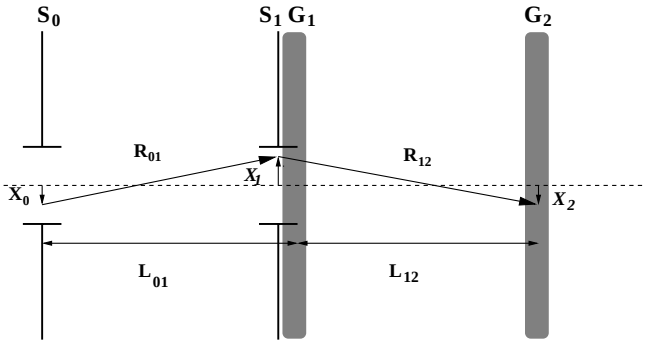

Fig. 2. Some notations used in the calculations of the diffracted amplitude. Analogous notations for paths between G_2 G_3 and D can be deduced easily from these ones.

where the notations are explained in Figure 2. The usual Fresnel approximations apply here and we can consider the R_{ij} as constant in the denominator and simplify their expression in the phase as follows

$$R_{ij} = \sqrt{L_{ij}^2 + (X_i - X_j)^2 + (Y_i - Y_j)^2} \simeq L_{ij} + \frac{(X_i - X_j)^2 + (Y_i - Y_j)^2}{2L_{ij}}. \quad (6)$$

In the Fraunhofer limit, we could neglect the phase associated with the wavefront curvature and in this case the phase would be a linear function of the various X_i. This limit holds if

$$\frac{k_a X_{max}^2}{2L} \ll 2\pi \quad (7)$$

whereas this quantity reaches values as large as 10π in the case of sodium waves (see Tab. 1) and a 10 μm wide slit S_1.

If the lines of the three gratings are perfectly parallel to the **y** axis defined in Figure 1 and if the dimension of the collimating slits along this axis are large, we can consider that no diffraction occurs in the **y** direction. The maximum Y values may still be small enough so that the phase associated with the neglected fourth order terms in equation (6) remains negligible. The integration over Y_1, Y_2 and Y_3 giving $A(\mathbf{R}_0, \mathbf{R}_4)$ can be done exactly using the results of Appendix A and the result depends on Y_0 and Y_4 by a phase which has no practical consequence (see Eq. (4)) and that we ignore. Then $A(\mathbf{R}_0, \mathbf{R}_4)$ reduces to $A(X_0, X_4)$

$$A(X_0, X_4) = A \int_{-e_1/2}^{e_1/2} dX_1 \int_{-\infty}^{\infty} dX_2 \int_{-\infty}^{\infty} dX_3 \times \exp\left(ik_a \sum_{j=1}^{4} \frac{(X_{j-1} - X_j)^2}{2L_{j-1,j}} \right) t(X_1) t(X_2) t(X_3) \quad (8)$$

where A stands for the constant term

$$A = A_0 \frac{1}{\sqrt{2\lambda^3}} \frac{e^{ik_a L_{04}}}{\sqrt{L_{04}}} (1+i) \frac{1}{\sqrt{L_{01} L_{12} L_{23} L_{34}}}. \quad (9)$$

We can expand the gratings transmission in a Fourier's series:

$$t_i(X_i) = \sum_{p_i=-\infty}^{\infty} \alpha_i(p_i) e^{ip_i k_g (X_i - x_i)} \quad (10)$$

where x_i measures the transverse position of grating G_i. $\alpha_i(p_i)$ is the amplitude diffracted in order p_i by the grating G_i and k_g is the common grating wavevector. The calculation of $\alpha_i(p_i)$ and its dependence with p_i is discussed in Appendix C.

The diffracted amplitude can now be expressed as a sum over different paths, defined by their successive diffraction orders p_1, p_2, p_3

$$A(X_0, X_4) = \sum_{p_1 p_2 p_3} e^{-ik_g(p_1 x_1 + p_2 x_2 + p_3 x_3)} \times \alpha_1(p_1)\alpha_2(p_2)\alpha_3(p_3) A_{p_1 p_2 p_3}(X_0, X_4) \quad (11)$$

where $A_{p_1 p_2 p_3}$ and $\Phi_{p_1 p_2 p_3}$ are defined as follows

$$A_{p_1 p_2 p_3}(X_0, X_4) = A \int_{-e_1/2}^{e_1/2} dX_1 \int_{-\infty}^{\infty} dX_2 \times \int_{-\infty}^{\infty} dX_3 e^{i\Phi_{p_1 p_2 p_3}} \quad (12)$$

$$\Phi_{p_1 p_2 p_3} = k_a \sum_{j=1}^{4} \frac{(X_{j-1} - X_j)^2}{2L_{j-1,j}} + k_g \sum_{j=1}^{3} p_j X_j. \quad (13)$$

Thanks to Appendices A and B, we can easily compute these integrals. The important result is that the diffraction amplitude due to diffraction by the slit S_1 is the same function of the coordinates X_0 and X_4 for all sets of diffraction orders. The effect of diffraction by the three gratings is only to shift this amplitude in space and in phase and to give to each set a different weight $\alpha_1(p_1)\alpha_2(p_2)\alpha_3(p_3)$

$$A_{p_1 p_2 p_3}(X_0, X_4) = e^{i\Psi_{p_1 p_2 p_3}} A_{000}(X_0, X_4') \quad (14)$$

where X_4' is given by

$$X_4' = X_4 - (p_1 L_{14} + p_2 L_{24} + p_3 L_{34})\theta. \quad (15)$$

The spatial shift $X_4 - X_4'$ depends only on the diffraction orders and the geometry of the apparatus. The phase shift $\Psi_{p_1 p_2 p_3}$ is given in Appendix B (B.6). We need to evaluate the function $A_{000}(X_0, X_4)$ which is just the amplitude in the detector plane of the wave emitted by the source at X_0 and diffracted by the slit S_1, as if there were no gratings. Its value is given below for sake of completion:

$$A_{000}(X_0, X_4) = A_0 \exp\left(ik_a \left(L_{04} + \frac{(X_4 - X_0)^2}{2L_{04}} \right) \right) \frac{(1-i)}{2L_{04}} A_d(X_1^*) \quad (16)$$

$$A_d(X_1^*) = \sqrt{\frac{2L_{04}}{\lambda L_{01} L_{14}}} \int_{-e_1/2-X_1^*}^{e_1/2-X_1^*} du \times \exp\left(ik_a \frac{u^2}{2}\left(\frac{L_{04}}{L_{01}L_{14}}\right)\right) \quad (17)$$

$$X_1^* = (L_{01}X_4 + L_{14}X_0)/L_{04}. \quad (18)$$

X_1^* is the point where the straight line going from X_0 to X_4 crosses the plane of the diffracting slit. In conclusion, our simulation reduces to the computation, for each set p_1, p_2, p_3 of diffraction orders, of the amplitude diffracted in X_4 from X_0, $A_{p_1,\,p_2,\,p_3}(X_0, X_4,)$ and the numerical integration has to be done only once as it is identical for any set p_1, p_2, p_3. The function $|A_{000}(X_0, X_4)|^2$ is plotted in Figure 3a, and clearly the Fresnel diffraction effects are very important.

If we consider only the two paths of Figure 1 and when the interferometer is perfectly symmetric ($L_{12} = L_{23}$), the diffraction amplitude A_{1-10} and A_{01-1} are identical functions of X_0 and X_4

$$I(X_0, X_4) \propto |A_d(X_1^*)|^2(1 + C_0 \cos(k_g(x_1 - 2x_2 + x_3))) \quad (19)$$

where C_0 depends only on the diffraction parameters $\alpha_j(p_j)$ and is equal to unity if the first and the third gratings are identical. This interference pattern keeps the same contrast C_0 when integrated over the source and detector width. However it is not obvious that one can put the detector in a region where only the two paths of Figure 1 contribute to the signal. This point is discussed in Section 5.

4 Defects of the interferometer

In this section, we consider two defects of the interferometer and we first assume a monochromatic source. In the first case, the distances between the gratings are not equal and in the second case, the gratings are slightly rotated in their plane. We still limit the discussion to an interferometer where only the two paths of Figure 1 are taken into account.

4.1 Mismatch of the distances between the gratings

We want to estimate the effect of the mismatch $\Delta L = L_{23} - L_{12}$ on the contrast. For simplicity, we introduce the classical phase $\Phi^{cl}_{p_1p_2p_3}$ associated with a path going from point source X_0, falling on detector point X_4 and undergoing successive diffraction of orders p_1, p_2, p_3

$$\Phi^{cl}_{p_1p_2p_3} = \Psi_{p_1p_2p_3} + k_a \frac{(X_4^{'} - X_0)^2}{2L_{04}}\,. \quad (20)$$

The two waves leaving X_0 and falling on X_4 encounter a phase difference $\Delta\Phi^{cl}$ proportional to the mismatch ΔL and which is given by

$$\Delta\Phi^{cl} = k_g \Delta L \left[\theta\left(\frac{\overline{L}}{L_{04}} - \frac{1}{2}\right) + \frac{X_0 - X_4}{L_{04}}\right] \quad (21)$$

where $\overline{L}$ is the mean value of L_{12} and L_{23}. Another phase difference is induced, due to the fact that the two diffraction patterns are no longer perfectly identical. There is no simple expression for this last term, but it plays a negligible role in the limit of a wide diffracting slit S_1. The phase difference given by (21) separates in a constant term which only induces a global phase shift of the interference pattern. This shift is compensated by translation of the third grating. The second term is proportional to $(X_0 - X_4)$ and can be compensated only on average. So the contrast decreases when integration over the source and detector areas is performed. If the only phase shift we consider is the classical one $\Delta\Phi^{cl}$, and if we ignore the one induced by modification of the two diffraction figures, the contrast would be reduced from its value C_0 corresponding to ΔL=0, to a new value C. This modification depends on the width e_0 of the source slit S_0, the width d of the detector and the period of the gratings through $k_g = 2\pi/a$:

$$C = C_0 \left|\mathrm{sinc}\left(\frac{k_g e_0 \Delta L}{2L_{04}}\right)\mathrm{sinc}\left(\frac{k_g d \Delta L}{2L_{04}}\right)\right| \quad (22)$$

where $\mathrm{sinc}(x) = \sin(x)/x$. Figure 4 compares this expression to the result of the numerical simulation which makes no approximation. The phase difference associated with the diffraction by the slit S_1 becomes negligible when this slit is wide enough and then equation (22) gives the same result as the numerical computation.

4.2 Grating rotation

Another imperfection of the interferometer which can be taken into account in our model is the rotation of the three gratings in their plane, *i.e.* $\mathbf{k}_{g_1}$, $\mathbf{k}_{g_2}$ and $\mathbf{k}_{g_3}$ keep the same norm, are still in the same plane $(\mathbf{x}, \mathbf{y})$ but have slightly different directions in this plane. Let δ_i be the angle between the vector $\mathbf{k}_{g_i}$ and the $\mathbf{x}$ axis. In this case, equation (5) remains true but we cannot ignore the $\mathbf{y}$ direction (see Fig. 1) as in equation (8). In a first order approximation in δ_i, the Fourier series now become

$$t_i(\mathbf{R}_i) = \sum_{p=-\infty}^{\infty} \alpha_i(p_i) e^{-ip_i \mathbf{k}_{g_i}\cdot\mathbf{r}_i} e^{ip_i k_{g_i}(X_i + \delta_i Y_i)}. \quad (23)$$

In this approximation, the integration over X_1, X_2 and X_3 is not affected but the integration over Y_1, Y_2 and Y_3 gives a different result, depending on Y_0 and Y_4. We consider that the slit height is such that we can neglect diffraction by the second slit S_1 along the $\mathbf{y}$ direction. With the same integration techniques of Appendices A and B, the calculations can be done in closed form. The angles δ_j induce a phase difference between the two arms. A part of this term is independent of Y_0 and Y_4 and does not induce any contrast loss. The other contribution to the phase difference depends linearly on Y_0 and Y_4. It induces a contrast loss when the signal is integrated over the height h_0 of the source slit S_0 and the height h_D of the detector.

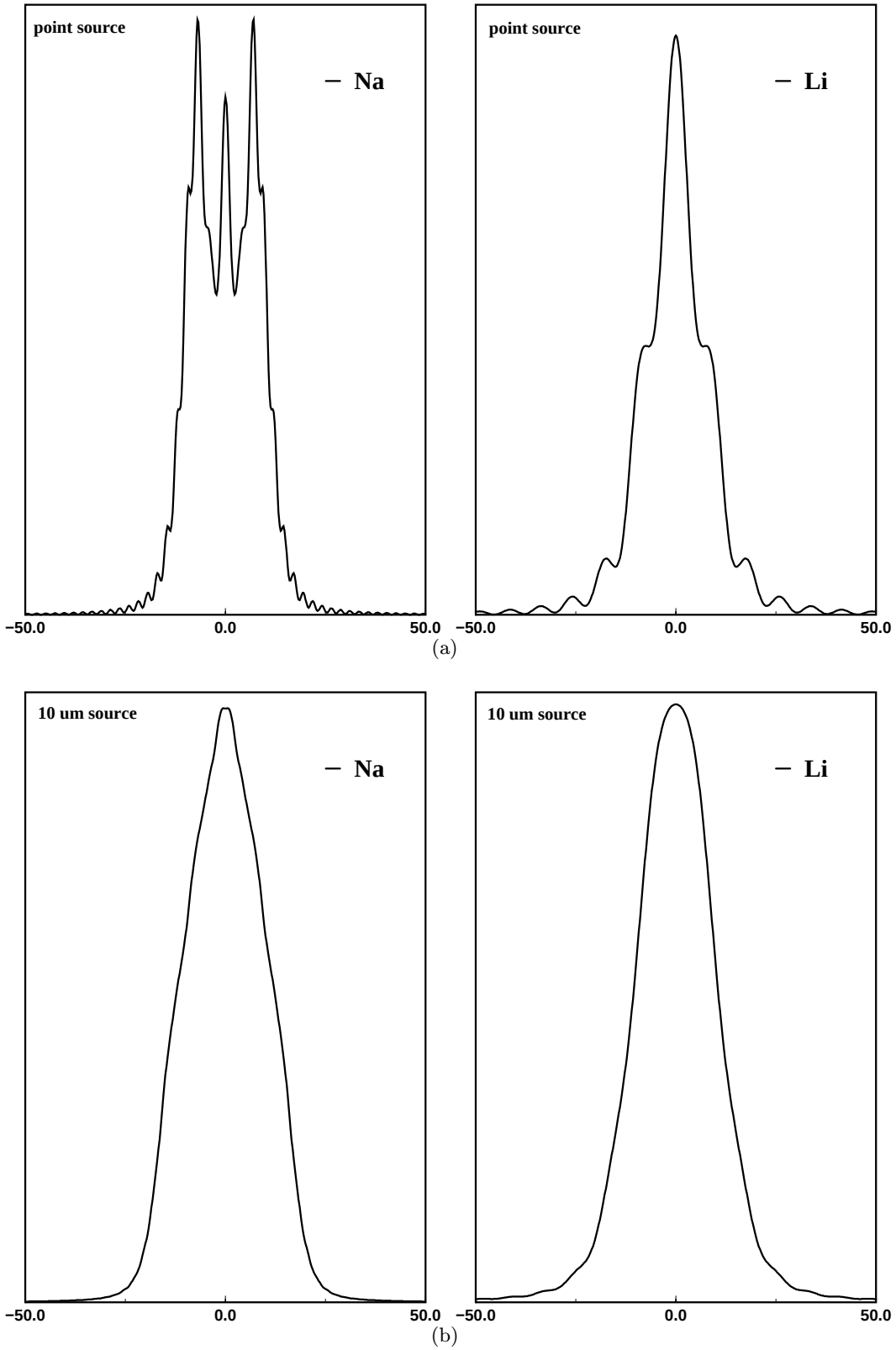

Fig. 3. (a) Intensity diffracted by slit S_1 in the detection plane in the case of a point source (left: sodium beam, right: lithium beam). (b) Intensity diffracted by the same slit S_1 in the case of a source slit S_0 of width $e_0 = 10$ μm. The slit S_1 has a width $e_1 = 10$ μm and the atomic velocity is 1000 m/s. The distance L_{14} from the slit S_1 to the detector plane is fixed at 1.4 m and the intensities are plotted *versus* X_4 expressed in μm.

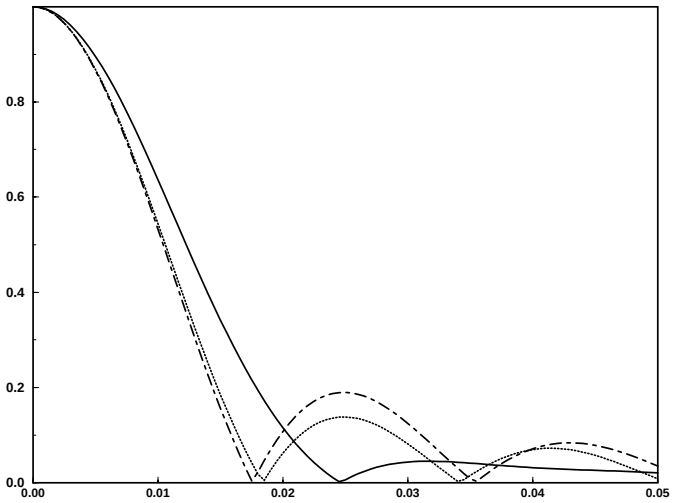

Fig. 4. Contrast of the fringe pattern *versus* mismatch $\Delta L = L_{23} - L_{12}$ in meters, for a lithium beam with a velocity equal to 1000 m/s and a grating period a equal to 335 nm. In the three cases the source width e_0 is 10 μm and the detector width d is 50 μm. The width of the collimating slit e_1 is 10 μm (solid line), 20 μm (dotted line) or 30 μm (dot-dashed line). The contrast calculated according to equation (22) is identical to the one computed in this last case as long as $\Delta L < 0.05$ m.

This contrast is now reduced from C_0 to

$$C = C_0 \left| \mathrm{sinc}\left[\frac{k_g h_0}{2}\left(\frac{\delta_{21}L_{14} + \delta_{23}L_{34}}{L_{04}}\right)\right] \times \mathrm{sinc}\left[\frac{k_g h_D}{2}\left(\frac{\delta_{21}L_{01} + \delta_{23}L_{03}}{L_{04}}\right)\right]\right| \quad (24)$$

where $\delta_{21} = \delta_2 - \delta_1$ and $\delta_{23} = \delta_2 - \delta_3$. This expression is just a generalization of the results presented in [7] to the case where the detector is not in the plane of the third grating. With a source and a detector having both a 1 mm height and a distance $L_{34} = 0.6$ m, the contrast has its first zero for $\delta_{23} = 435$ μrad for a lithium interferometer and 258 μrad for a sodium interferometer (all other parameters as in Tab. 1). This implies that the gratings must be parallel to better than a few tens μrad.

The two analytic expressions (Eqs. (22, 24)) for the contrast show that smaller grating periods render the contrast more sensitive to misalignment.

4.3 A non monochromatic source

In the case of a polychromatic source, phase shifts induced by these different defects suffer from dispersion and the contrast of the fringes is further reduced. Usually the longitudinal velocity distribution can be approximated by a Gaussian as long as this distribution is sufficiently narrow (*i.e.* $\alpha \ll u$) [9]

$$P(v) = \frac{1}{\sqrt{\pi}\alpha} e^{-((v-u)/\alpha)^2} \quad (25)$$

where α is related to the longitudinal temperature of the atomic beam. The coherence length of such a source l_c is [10]:

$$l_c = \frac{\lambda_0}{\sqrt{2}\pi}\frac{u}{\alpha}\,. \quad (26)$$

We define the mean wavelength λ_0 as the value of λ for $v = u$ and in a similar way, we call θ_0 the corresponding value of the diffraction angle θ. The finite coherence length reduces the contrast of a two beams interference pattern in the following way:

$$C(\xi) = C_0 e^{-\xi^2/(2l_c)^2} \quad (27)$$

where ξ is the difference in optical paths and C_0 is the contrast for $\xi = 0$.

When the distances between the gratings are different, the loss of contrast associated with this dispersion can be evaluated as in Section 4.1 if it is a good approximation to neglect the phase differences induced by the different diffraction amplitudes by slit S_1. Then, if C is the contrast for a monochromatic source, the contrast becomes

$$C' = C \exp\left(-\left(\frac{k_g \Delta L}{2}\left(\frac{\overline{L}}{L_{04}} - \frac{1}{2}\right)\frac{\alpha}{u}\theta_0\right)^2\right). \quad (28)$$

The contrast is now a decreasing function of $k_g\theta_0 = 2\pi\lambda/a^2$ and not of $1/a$ as in equation (22). Therefore, the best compromise between a large diffraction angle and a small sensitivity to defects is to choose a large atomic wavelength and a large grating periodicity.

The calculation of the fringe contrast can be also performed by a numerical average over the velocity distribution (25). As expected, the numerical result agrees very well with the analytical expression for cases where the phase effect of the diffraction by the slit S_1 is negligible (for instance $e_1 = 30$ μm and $\Delta L \leq 0.05$ m as in Fig. 4). When this phase effect cannot be neglected, the calculated contrast decreases faster with ΔL than the analytical result.

In case of rotation of the gratings, the expression of the new contrast is similar to equation (28) but the terms appearing in the exponential are proportional to δ_i^2 and we may expect that the corresponding loss of contrast will be small. In any case, as we have carried the calculations only up to the first order in δ_i, it is not reasonable to discuss only one second order effect.

5 Contribution of multiple paths to the signal

When diffraction is performed by a standing laser wave (*i.e.* a phase grating) or with a material grating (*i.e.* an amplitude grating), simultaneous diffraction in several orders is obviously possible and has been observed [3]. So the paths represented in Figure 1 are not the only ones which may contribute to the signal. This problem does not occur when the laser wave is thick enough so as to play the

Table 2. FWHM (in μm) of diffraction in the detector plane image of a 1000 m/s atomic beam of lithium and sodium for different widths of source and collimating slits. $L_{12} = L_{23} = L = 0.6$ m and $L_{34} = 0.6$ m.

atom	diffracting slit	point source	10 μm wide source	20 μm wide source	θL
Li	10 μm	26	26	48	97 μm
Li	20 μm	51	58	58	97 μm
Na	10 μm	25	32	46	49 μm
Na	20 μm	56	59	59	49 μm

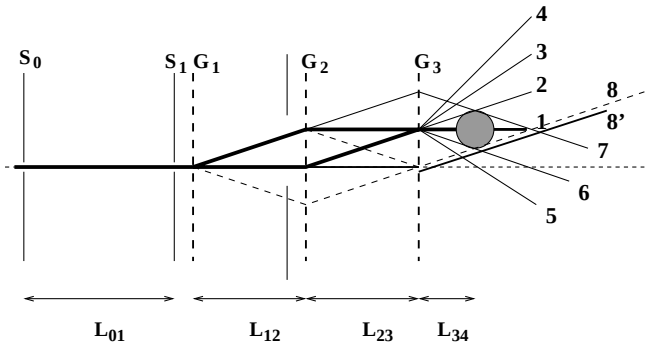

Fig. 5. Diffracted paths that contribute the most to the signal. The coherence groups labeled on the figure are defined by their diffraction orders as follows: group 1: 1, −1, 0 and 0, 1, −1; group 2: 1, −1, 1 and 0, 1, 0; group 3: 1, −1, 2 and 0, 1, 1; group 4: 1, −1, 3 and 0, 1, 2; group 5: 1, −1, −2 and 0, 1, −3; group 6: 1, −1, −1 and 0, 1, −2; group 7: 1, 0 , −2; group 8: 1, −2, 2 and −1, 2, 0; group 8': 0, 0, 1.

role of a crystal for the atomic wave. Then, diffraction occurs only if the Bragg matching condition is fulfilled. This condition allows only one diffraction angle [4,11] if the longitudinal velocity dispersion is not too wide [12] and in an interferometer using Bragg diffraction, the two-path description should be valid. Then the theoretical contrast can be as large as 100%. Indeed, the observed contrast in the experiment done in Siu Au Lee's group [5] has reached the quite good value of 62% although the atoms were not optically pumped.

In this section, we focus on the effect of extra diffracted paths on the fringe contrast, such as illustrated in Figure 5. We now suppose the interferometer perfectly aligned ($\mathbf{k}_{g_i} = \mathbf{k}_g$) and balanced ($L_{23} = L_{12}$). We compare the interferometer we want to build using a lithium beam and phase gratings (PG) with periodicity $a = \lambda_L/2 =$ 335 nm to the only existing amplitude gratings (AG) interferometer, the one built by Pritchard's group, using a sodium beam [13]. We will use in the calculations the value of the grating period $a = 200$ nm [2] although smaller values also have been used [14].

The contribution of extra beams can be very important, depending on the widths of the detector and of the slits. The intensities diffracted in the detector plane by a 10 μm slit from a 10 μm wide source are plotted in Figure 3b and Table 2 sums up the FWHM of these intensities for sodium and lithium as well as for different slit widths. It is useful to compare these widths to the transverse shift θL between consecutive exiting paths. This comparison proves that many paths can contribute to the signal. As a consequence, L_{34} must be chosen to minimize these effects and the detector and slit widths must be adjusted so as not to waste any signal.

5.1 Coherence

Multiple paths can fall on the detector but not all of them give observable interference signals after integration over the detector surface. In the calculation, we take into account the interference effect only between coherent beams and we add the intensities resulting from various "groups of coherence". Practically, two or several paths are coherent and can interfere if they exit the last grating with the same transverse position and direction. Moreover, to be realistic, we must take into account the finite coherence length of the source.

Since a Mach-Zehnder interferometer exhibits white fringes for identical optical paths (like the (0 +1 −1) and (+1 −1 0) ones), all the atoms of the same path form the same interference pattern regardless of their velocity. As a consequence, in most part of our simulations we neglect the effect of longitudinal velocity dispersion on the interference pattern. But this dispersion must be taken into account to select coherent paths. For a beam of average velocity $u = 1000$ m/s and a velocity dispersion (FWHM) of 10%, $l_c = 3.7\lambda$ comparable to 1 or 2 Å whereas the optical path difference between two non symmetric paths is a multiple of $L\theta^2$ which is 170 Å for lithium and 40 Å for sodium, more than an order of magnitude greater than l_c. As a consequence, if two paths do not have exactly the same length, $\xi \gg l_c$ and they are not coherent. If the two paths have the same length, they belong to the same group $\{g\}$ of coherence and with the preceding notations and according to (4), the intensity on the detector point X_4 is

$$I(X_0, X_4) = \sum_g I(X_0, X_4, \{g\})$$

with

$$I(X_0, X_4, \{g\}) = |\sum_{p_1,\, p_2,\, p_3 \in \{g\}} A_{p_1,\, p_2,\, p_3}(X_0, X_4)|^2. \quad (29)$$

5.2 Comparison between phase and amplitude gratings

The detection with an amplitude-grating (AG) interferometer can be described [7] as a Moiré detection where the last grating filters an atomic wave resulting from interference of the two paths of Figure 1 and which is stationary in the transverse direction **x**. This description is not the only relevant one and indeed does not explain the interference pattern obtained with phase gratings (PG). In this case, there is no Moiré effect and a detector very close to the third grating measure a fringe pattern with a zero contrast.

Figure 6 illustrates how we can explain these differences between these two types of interferometers, with our model. For AG, since all the diffraction amplitudes are real positive (*cf.* Appendix C), all the major exiting paths give fringe patterns which are in phase. In the PG case, however, some are in phase opposition because of the negative or imaginary nature of some of the diffraction amplitudes (*cf.* Appendix C). In the PG case, setting the detector further away from the last grating allows discrimination against opposite phase contributions and accordingly the contrast increases when L_{34} increases. For the AG case, the detection evolves from a Moiré detection (L_{34}=0) where all diffraction orders from the last grating contribute, to a "symmetric interferometer" detection where these orders separate and only some of them contribute to the signal. In the Moiré detection scheme, the fringe contrast is given by:

$$C = \frac{\sin(\pi\beta_3)}{\pi\beta_3} C_0 \tag{30}$$

where C_0 is the contrast of the atomic standing wave in the plane of the third grating and β_3 the clear fraction of the third grating G_3. This contrast can never reach 100% even in the absence of extra paths (except if $\beta \to 0$, but this would reduce the signal to zero). But as soon as the paths diffracted by the last grating separate in the plane of the detector, the signal is comparable to the one obtained with a phase grating interferometer.

Figure 7 proves that the location of the detector should not be the same for amplitude and phase gratings, but that for a good choice of the distance L_{34} between the third grating G_3 and the detector, the best theoretical contrast can be as large as 80% in both cases. Of course the width of the detector and of the slits are very important and the maximum contrast drops from 81% to 54% for the sodium AG interferometer with $\beta = 0.33$ and from 93% to 74% for the lithium PG interferometer when we simultaneously increase the width of the detector from 50 μm to 100 μm and the width of the two slits from 10 to 20 μm.

Using a 50 μm wide detector and 10 μm slits, we can improve the contrast by using another exiting path of the interferometer (labeled 2 in Fig. 5). It gives a worse contrast for a PG interferometer using lithium but leads to a better contrast for large distance L_{34} in case of an AG interferometer. One should be aware that the interference patterns observed on these two exits have phase opposition but not exactly the same intensities. Zeilinger's group [6] used this complementary exit to improve the contrast of their PG interferometer using metastable argon. They obtained better contrast in this case because they used the exit labeled 1 only for small values of the distance L_{34} between detector and third grating, a choice which is not appropriate to this kind of diffraction. With their design and using the exit labeled 1, the calculated contrast reaches a very good value for distance L_{34} larger than 0.6 m ($C = 76\%$). For the exit labeled 2, the calculated contrast is slightly less good (65%) at $L_{34} = 0.75$ m.

The sensitivity of the contrast to a mismatch of the distances between the gratings is now different from the simple case considered in Section 4.1. In this paragraph, we limited our discussion to the two paths of Figure 1. In the more general case of a multipath interferometer, the phase difference $\Delta\Phi^{cl}$ induced by $\Delta L = L_{23} - L_{12}$ between the paths inside a group of coherence still separates into a constant term and a term depending on X_0 and X_4 as in equation (21). The dependence of this second term with X_0 and X_4 appears to be identical for all the studied groups of coherence, but the first term behaves differently for the various groups of coherence. As a consequence, the global phase shift induced on the interference patterns by these constant terms is different for the various groups of coherence. These phase shifts also contribute to the loss of contrast if the interference patterns are in phase when the interferometer is well-balanced ($\Delta L = 0$). It is true for all groups in an AG interferometer and only for some of them in a PG one. For the other ones, the interference patterns are exactly in phase opposition when $\Delta L = 0$ so the mismatch will reduce this dephasing and the fringe contrast could increase.

5.3 Dependence with the transverse position of the detector

The contribution of all the extra paths explains the existence of an optimum longitudinal position for the detector, when its transverse position remains fixed. They explain too the variations of the observed contrast with the transverse position of the detector when its longitudinal one is kept fixed. We analyze this behaviour for the longitudinal position where the contrast is maximum ($L_{34} \simeq 0.11$ m for Na and AG and $L_{34} \simeq 0.35$ m for Li and PG) and for a position of the detector center x_D varying by $\pm\, \theta L/2$ around the position of the principal exit $x_D = \theta L$. The results of these calculations are shown in Figure 8. As expected, the contrast reaches its maximum very close to the position of the principal exit but the shape of the two curves are very different. A phase inversion of the fringe pattern for $x_D \simeq 120$ μm explains the shape of the calculated contrast for a lithium beam and PG. This inversion is due to a change of the main contributing path. For positions of the detector around $x_D = \theta L + \theta L/2$, the path with the largest contribution to the signal is the one labeled 2 in Figure 5. The fringe pattern due to this path is in phase opposition with the main one (labeled 1) for PG but in phase with it for AG.

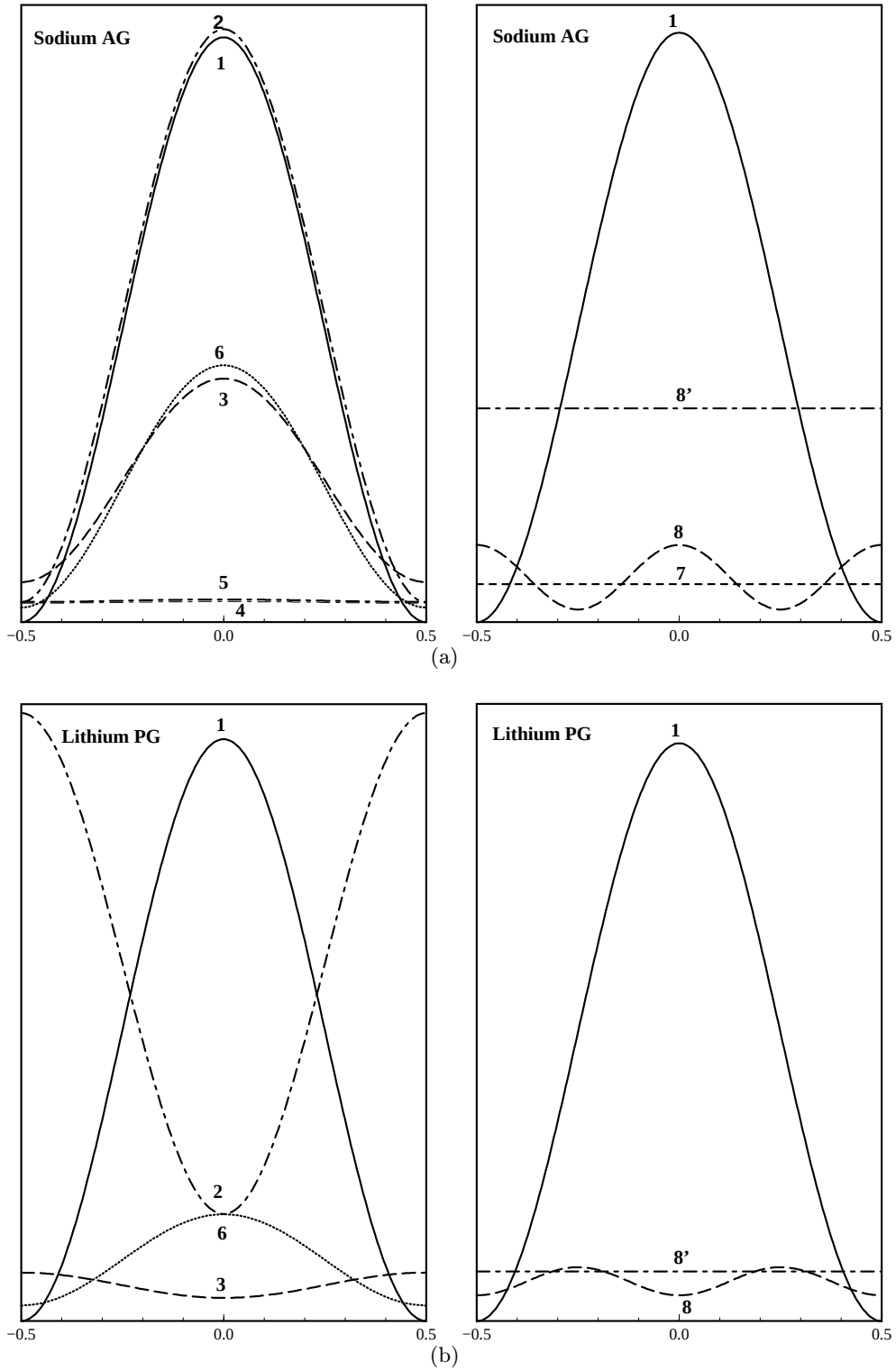

Fig. 6. (a, b) Contribution to the interference pattern of the most intense paths *versus* the displacement x_3 of the third grating, measured in units of the grating period a. The calculations are made for the two kinds of interferometer ((a): sodium and amplitude gratings with $\beta = 0.33$, (b): lithium and phase gratings) and two extreme positions of the detector (left: $L_{34} = 0.1$ m, right: $L_{34} = 0.6$ m). The paths are labeled according to the coherence groups labeled as in Figure 5. $e_0 = e_1 = 10$ μm and $d = 50$ μm and the transverse position of the detector is in front of the beam labeled 1 in Figure 5 ($x_D = \theta L$).

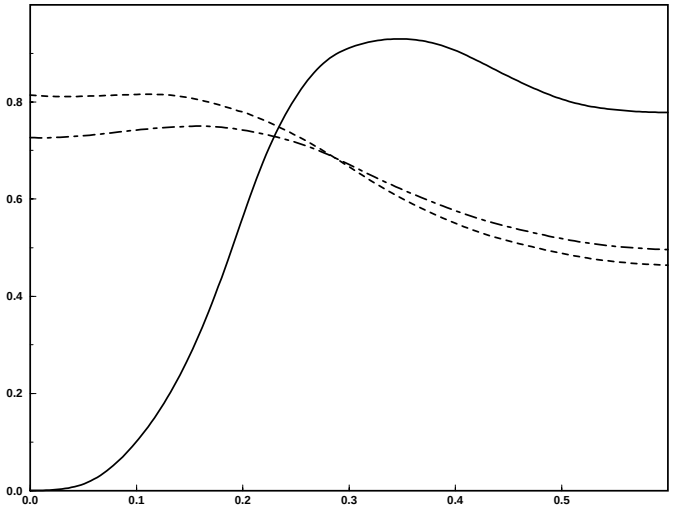

Fig. 7. Contrast of the fringe pattern *versus* position of the detector L_{34} (m). Solid line: lithium beam and phase gratings, dashed line: sodium beam with amplitude gratings $\beta = 0.33$, dot-dashed line: *idem* $\beta = 0.4$. In the three cases, calculations are done with $e_0 = e_1 = 10$ μm and $d = 50$ μm. The transverse position of the center x_D of the detector is in front of the beam labeled 1 in Figure 5 ($x_D = \theta L$).

6 Conclusion

In this paper, we have reanalyzed the Fresnel-Kirchoff theory of the three grating Mach-Zehnder interferometers. We have simplified the multiple integrals by analytical means so that the interferometer signal is obtained thanks to a modest computational effort.

We have thus been able to analyze the fringe contrast and its reduction when the interferometer is not well-aligned. This calculation has been done in the case of a monochromatic source as well as in the more realistic case of an atomic beam with a Gaussian velocity distribution. Analytical formulae have been given which explain the contrast reduction as a function of the alignment defects in many important cases.

We have also clarified the relation between Moiré detection which is possible only with amplitude gratings and the normal Mach-Zehnder interfering paths detection which is the only possible scheme for phase gratings.

We would like to thank Bertrand Georgeot for helpful discussions on the classical phase approximation, Christian Girard for informations on the atom-surface interactions and John Weiner for a critical reading of the manuscript. We thank Région Midi-Pyrénées for financial support of our laboratory.

Appendix A: Diffraction by an infinite plane

In many occasions we have to evaluate integrals of the type

$$\Im = \int_{-\infty}^{+\infty} dX_j \times \exp\left(ik\left(\frac{(X_j - X_{j-1})^2}{2M} + \frac{(X_{j+1} - X_j)^2}{2N}\right)\right). \quad \text{(A.1)}$$

The important point is that this integral is not limited in the X_j plane which means that no diffraction occurs in the jth plane. The calculation is made easier by the introduction of the ray defined by the stationary phase condition and going from X_{j-1} to X_{j+1} through X_j^*. This stationary point X_j^* is defined by the ray equation

$$\frac{X_j^* - X_{j-1}}{M} - \frac{X_{j+1} - X_j^*}{N} = 0. \quad \text{(A.2)}$$

By the change of variable $u = X_j - X_j^*$ the integral (A.1) reduces to a standard Fresnel integral and the result is

$$\Im = (1+i)\sqrt{\frac{\pi}{k}\left(\frac{MN}{M+N}\right)} \times \exp\left(\frac{ik(X_{j-1} - X_{j+1})^2}{2(M+N)}\right). \quad \text{(A.3)}$$

The equality between (A.1) and (A.3) expresses the clear physical equality between free propagation from plane $j-1$ to plane $j+1$ and propagation through a infinite diffractive plane j placed between $j-1$ and $j+1$.

Appendix B: Calculation of the diffracted amplitude

We want to simplify equation (8)

$$A_{p_1p_2p_3}(X_0, X_4) = \int_{-e_1/2}^{e_1/2} dX_1 \int_{-\infty}^{\infty} dX_2 \int_{-\infty}^{\infty} dX_3 e^{i\Phi_{p_1p_2p_3}} \quad \text{(B.1)}$$

where

$$\Phi_{p_1p_2p_3} = k_a \sum_{j=1}^{4} \frac{(X_j - X_{j-1})^2}{2L_{j-1,j}} + k_g \sum_{j=1}^{3} p_j X_j. \quad \text{(B.2)}$$

We recall that e_1 is the width of slit 1 and that contrary to X_2 and X_3, the integration over X_1 is limited by this width. The second order expansion on X_j (*cf.* Eq. (6)) is obviously not valid for large X_j but it is valid in the region around the stationary path, where the main contribution to the integral is located. We then make a change of variables such that the stationary path becomes a straight line. Two different changes can be made, either on X_1, X_2, X_3 or on X_2, X_3, X_4. We present here the latter which has a simpler physical meaning as it compensates exactly the shifts induced by the diffraction gratings:

$$\begin{aligned} X_0' &= X_0 \\ X_1' &= X_1 \\ X_2' &= X_2 - (p_1 L_{12})\theta \\ X_3' &= X_3 - (p_1 L_{12} + (p_1+p_2)L_{23})\theta \\ X_4' &= X_4 - (p_1 L_{12} + (p_1+p_2)L_{23} + (p_1+p_2+p_3)L_{34})\theta. \end{aligned} \quad \text{(B.3)}$$

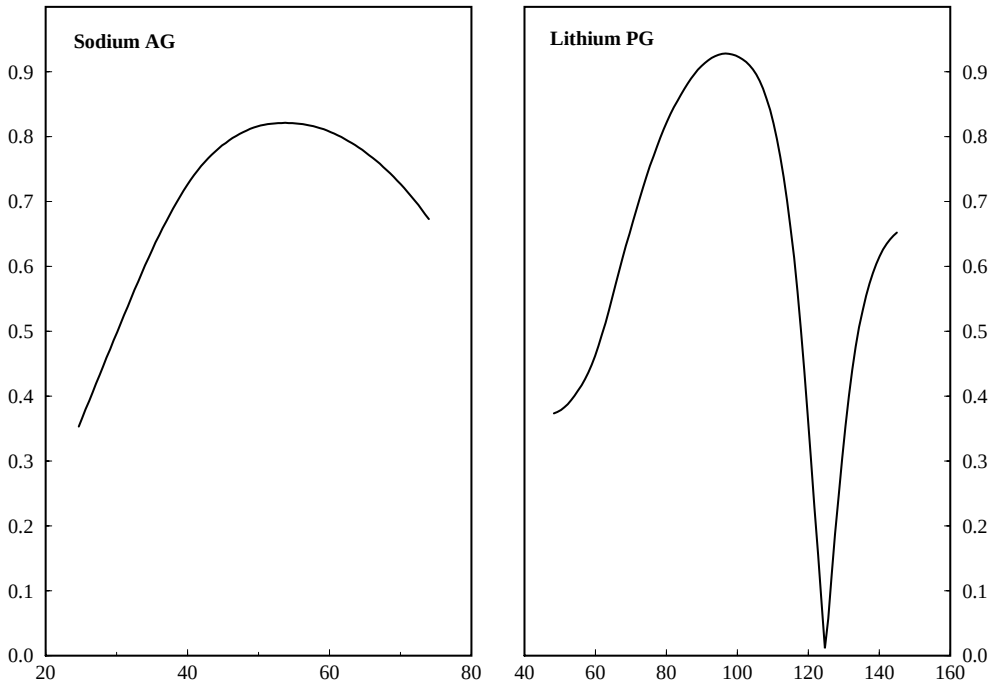

Fig. 8. Contrast of the fringe pattern for the sodium AG (left) and lithium PG (right) interferometers, *versus* the position of the center of the detector x_D (μm). The longitudinal position L_{34} of the detector is 0.11 m for the sodium interferometer and 0.35 m for the lithium one *i.e.* the values which give the best contrast. The calculations are done with the slit widths $e_0 = e_1 = 10$ μm and a detector width $d = 50$ μm.

With these new variables $\Phi_{p_1p_2p_3}$ expresses as

$$\Phi_{p_1p_2p_3} = k_a \sum_{j=1}^{4} \frac{(X_j^{'} - X_{j-1}^{'})^2}{2L_{j-1,j}} + \Psi_{p_1p_2p_3} \qquad \text{(B.4)}$$

the supplementary phase $\Psi_{p_1p_2p_3}$ which depends only on $X_4^{'}$ is discussed below. When using twice the result of Appendix A, the integrals on $X_2^{'}$ and $X_3^{'}$ variables are easily done. Finally, we use for X_1 the same change of variable as in Appendix A but we cannot perform the integration because of the finite bounds

$$A_{p_1p_2p_3}(X_0, X_4) = e^{i\Psi_{p_1p_2p_3}} \exp\left(\frac{ik_a(X_4^{'} - X_0)^2}{2L_{04}}\right) \times \int_{-e_1/2-X_1^*}^{e_1/2-X_1^*} du \exp\left(\frac{ik_a u^2 L_{04}}{2L_{01}L_{14}}\right) \qquad \text{(B.5)}$$

where X_1^* defines the straight line between X_0 and $X_4^{'}$ in the plane of the diffracting slit. We recognize here the diffraction pattern of the slit S_1 in the detector plane, simply shifted by $X_4 - X_4^{'}$ as a result of the diffraction by the gratings. There is also a phase shift $\Psi_{p_1p_2p_3}$ which, expressed with X_4, is

$$\Psi_{p_1p_2p_3} = (p_1 + p_2 + p_3)k_g X_4 - \frac{k_g\theta}{2}(p_1^2 L_{12} + (p_1 + p_2)^2 L_{23} + (p_1 + p_2 + p_3)^2 L_{34}). \qquad \text{(B.6)}$$

The first term expresses that the atomic wave has a component of its wavevector along the **x** direction equal to $(p_1 + p_2 + p_3)k_g$. The second term is a phase shift due to the modification in the optical paths.

Appendix C: The diffraction gratings

Phase and amplitude gratings have been used as beam splitters. Amplitude gratings are made of a periodic array of slits. These gratings are completely defined by their period a and their clear fraction β, or the width of the slits βa (in the simulation we use $\beta = 0.33$ or 0.4, according to [2]) and the diffraction amplitude in the pth order is given by

$$\alpha(p) = \frac{\sin(p\pi\beta)}{p\pi}\,. \qquad \text{(C.1)}$$

This expression only takes into account the amplitude effect of the slits and neglects the phase effect resulting from the van der Vaals interaction between the atoms of the beams and the wires of the gratings (gold or silicon nitride [2]). This phase effect will be discussed in the Appendix D.

Phase gratings consist of near-resonant standing waves which induce a periodical phase shift on the atomic wave due to the dynamical Stark effect. For a thin laser wave the motion of the atoms across this wave can be neglected, this is the Raman-Nath regime where the Kapitza-Dirac effect occurs [15]. In this case, the diffracted amplitude is

$$\alpha(p) = (i)^{|p|} J_{|p|}(\phi) \qquad \text{(C.2)}$$

where J_p is the pth Bessel function and ϕ a phase depending on the standing wave [15]. For large detuning δ between laser frequency and atomic transition

$$\phi = \frac{1}{2\delta}\int_{-\infty}^{+\infty} \Omega^2(t)dt \tag{C.3}$$

where $\Omega(t)$ is the local Rabi angular frequency of one traveling wave in the atom frame. If the laser electric field has a Gaussian transverse distribution in the atom local frame, $E(t) = E_0 e^{-(t/\tau)^2}$ where $\tau = \omega/v$ and

$$\phi = \frac{1}{2}\sqrt{\frac{\pi}{2}}\frac{\Omega_0^2\tau}{\delta} \tag{C.4}$$

where Ω_0 is the maximum Rabi pulsation of one traveling wave and ω its waist.

A striking difference between the two equations (C.1, C.2) is that the diffraction amplitudes are all real and positive in the first case while they can also be negative or imaginary in the second case. This difference has important consequences on the fringe contrast as discussed in Sections 5.2 and 5.3.

In a symmetric geometry where the first and third gratings play the symmetric role of beam splitters and the second one the role of mirrors, the contrast is optimum if ϕ_1 and ϕ_3 (or β_1 and β_3) are equal. Moreover the signal is maximum if they both maximize $|\alpha_1(0)\alpha_1(1)|$ ($\phi_1 = 1.08$ or $\beta_1 = 0.65$) whereas ϕ_2 (β_2) maximizes $|\alpha_2(1)|$ ($\phi_2 = 1.79$ or $\beta_2 = 0.5$). In our simulation, we choose for the ϕ_j these optimal values whereas the β_j are the ones measured experimentally by Pritchard's group.

Appendix D: Phase effects in material gratings

The van der Waals interactions between the atoms of the beam and the material of the slits of the gratings induce a phase effect which has been neglected so far. This effect can modify the diffraction amplitude $\alpha(p)$ associated to each diffraction order p. In this appendix we estimate this effect for a gold and a silicon grating.

We consider an interaction potential between an atom and the two plane surfaces constituting a slit. The clear aperture of the slit is still βa and we call l its thickness (along $\mathbf{z}$). If we neglect the finite size effect related to the finite thickness of the slit, this interaction behaves roughly like

$$V(x,z) = \begin{cases} -\left(\dfrac{C_3}{x_1^3} + \dfrac{C_3}{x_2^3}\right) & \text{if } 0 \le z \le l \\ 0 & \text{elsewhere} \end{cases} \tag{D.1}$$

where x_1 and x_2 are the distance between the atom and the two surfaces of the slit. If we consider that the atomic trajectory is not perturbed by this interaction, in a semi-classical approximation, the phase induced on the atomic wave by the constant potential $V(x)$ is

$$\Delta\Phi = \frac{Vl}{\hbar v_a}\cdot \tag{D.2}$$

The C_3 coefficients have been evaluated thanks to [16] for a sodium-gold ($C_3 = 1.20$ au) and a sodium-silicon ($C_3 = 1.11$ au) interaction. For a thickness l equal to 200 nm [2,17] the phase for an atom crossing the middle of the slit ($x_1 = x_2 = \beta a/2$ where β is the clear fraction) at a velocity $v = 1000$ m/s is 0.31 rad for the first case and 0.29 rad in the second case. This phase increases very rapidly when the atomic trajectory is closer to one side of the slit. This phase effect is obviously not negligible and it should be taken into account in a detailed description of the diffraction by material gratings. We have not tried to do so in the present work.

References

1. J. Schmiedmayer, C. Ekstrom, M. Chapman, T. Hammond, D. Pritchard, J. Phys. II France **4**, 2029 (1994).
2. C. Ekstrom, D. Keith, D. Pritchard, Appl. Phys. B **54**, 369 (1992).
3. P. Moskowitz, P. Gould, S.R. Atlas, D. Pritchard, Phys. Rev. Lett. **51**, 370 (1983).
4. P. Martin, B. Oldaker, A. Miklich, D. Pritchard, Phys. Rev. Lett. **60**, 515 (1988).
5. D. Giltner, R. McGowan, S.A. Lee, Phys. Rev. Lett. **75**, 2638 (1995).
6. E. Rasel, M. Oberthaler, H. Batelaan, J. Schmiedmayer, A. Zeilinger, Phys. Rev. Lett. **75**, 2633 (1995).
7. J. Schmiedmayer *et al.*, Optics and interferometry with atoms and molecules, in *Atom Interferometry*, edited by P. Berman (Academic Press, 1997), p. 1.
8. Q. Turchette, D. Pritchard, D. Keith, J. Opt. Soc. Am. B **9**, 1601 (1992).
9. H. Haberland, U. Buck, M. Tolle, Rev. Sci. Instrum. **56**, 1712 (1985).
10. C. Adams, M. Siegel, J. Mlynek, Phys. Rep. **240**, 143 (1994).
11. D. Giltner, R. McGowan, S.A. Lee, Phys. Rev. A **52**, 3966 (1995).
12. D. Giltner, Ph.D. thesis, Colorado State University, Fort Collins, 1996.
13. D. Keith, C. Ekstrom, Q. Turchette, D. Pritchard, Phys. Rev. Lett. **66**, 2693 (1991).
14. T. Hammond, Ph.D. thesis, Massachusetts Institute of Technology, 1997.
15. P. Gould, G. Ruff, D. Pritchard, Phys. Rev. Lett. **56**, 827 (1986).
16. X. Pjang, F. Toigo, M. Cole, Surf. Sci. **145**, 281 (1984).
17. D. Keith, M. Schattenburg, H. Smith, D. Pritchard, Phys. Rev. Lett. **61**, 1580 (1988).